Applied Surface Science 258 (2012) 8704–8712

Contents lists available at SciVerse ScienceDirect

Applied Surface Science

journal homepage: www.elsevier.com/locate/apsusc

Preparation and characterization of $SnO_2/ZnO/TiO_2$ composite semiconductor with enhanced photocatalytic activity

Guidong Yang[a,b,c], Zifeng Yan[b,*], Tiancun Xiao[c,**]

[a] Department of Chemical Engineering, State Key Laboratory of Multiphase Flow in Power Engineering, Xi'an Jiaotong University, Xi'an 710049, China
[b] State Key Laboratory for Heavy Oil Processing, China University of Petroleum, Qingdao 266555, China
[c] Department of Chemistry, Inorganic Chemistry Laboratory, University of Oxford, Oxford OX1 3QR, UK

ARTICLE INFO

Article history:
Received 4 February 2012
Received in revised form 15 May 2012
Accepted 15 May 2012
Available online 23 May 2012

Keywords:
Composite semiconductor
Heterojunction
Visible light
SnO_2
ZnO
TiO_2
Photocatalyst

ABSTRACT

In this study, $SnO_2/ZnO/TiO_2$ composite photocatalysts were successfully synthesized using sol–gel and solid-state methods. The as-prepared samples were characterized for the phase structure, optical absorption, thermal stability and surface property using X-ray diffraction (XRD), Raman spectroscopy, UV–vis diffuse reflectance spectra (DRS), X-ray photoelectron spectroscopy (XPS), thermogravimetric analysis (TGA) and scanning electron microscopy (SEM). The photocatalytic activity was tested with photodecomposition of Methyl Orange under both visible and UV light irradiations. The results indicated that the $SnO_2/ZnO/TiO_2$ composite materials have an apparent visible light absorption, combining TiO_2 with SnO_2 and ZnO could promote the TiO_2 phase transition from anatase to rutile. The $SnO_2/ZnO/TiO_2$ heterojunctions with the highest performance was the one prepared using Sn(Zn)/Ti molar ratio of 0.05. It was found that the enhanced photocatalytic activity could be attributed to the increased separation of the charge carriers, which therefore depress the charge pair recombination and prolonged the electron lifetime in the composite structure, and a large number of electrons could take part in the photoreaction. Based on the results of the present study, a tentative mechanism for the enhanced photocatalysis of the $SnO_2/ZnO/TiO_2$ composite catalyst has been proposed.

1. Introduction

Combining some semiconductors with different band gaps to form heterojunctions in photocatalytic systems has become a primary focus of researchers in recent year because of their somewhat unique properties not existed in the individual nanomaterial arising from the interfacial interaction at the nanoscale [1–5]. For example, it can efficiently reduce the recombination rate of the photogenerated charge carriers in the use of environmental purification and remediation. It also can significantly enhance the optical adsorption of photocatalyst [1–5].

TiO_2 [6], SnO_2 [7] and ZnO [8,9], as three well-known semiconductors, have been intensively investigated in the fields of photocatalysis, solar cell and gas sensors due to their special electronic and optical properties. Among these, TiO_2-based photocatalysts received more attention because of the peculiarities of high photo-oxidization, photostablility, low cost and non-toxicity [10–12]. However, with the wide band gap (~3.2 eV), TiO_2 shows a weak photoresponse to the visible light region, as well as a high electron (e^-)–hole (h^+) pairs recombination rate greatly reducing the quantum efficiency, both of which limited the further widespread application of TiO_2 for solar energy conversion, environmental cleanup and hydrogen generation [10–14]. With the purpose of decreasing the recombination of photogenerated charge carriers and improving the photocatalytic efficiency of TiO_2, considerable efforts have been devoted to develop highly active titanium dioxide photocatalysts by doping, metal deposition, surface sensitization and coupling of semiconductors [13,14]. The latter, in particularly, is thought to be the most promising technology for increasing the electron–hole pair separation efficiency to enhance the quantum yield of TiO_2, and the corresponding photocatalyst has been proven to perform well in the photocatalysis [15–19].

Tin dioxide (SnO_2) is a direct wide-band-gap semiconductor with a band gap of ~3.8 eV, which has no absorption of light with a wavelength longer than 330 nm [7]. In fact, the quantum efficiency of SnO_2 is quite low, however, such material may have a merit regarding their band structures. It is well known that the conduction band (CB) of SnO_2 is lower than that of TiO_2, but the valence band is higher than that of TiO_2, when coupled with titanium dioxide, its band gap is well matching the band levels with TiO_2, and this leads to the enhancement of the photocatalytic activity of coupling semiconductor under visible light [17–19]. Zinc

* Corresponding author. Tel.: +86 532 86981296; fax: +86 532 86981295.
** Corresponding author. Tel.: +44 1865 272660; fax: +44 1865 272690.
E-mail addresses: zfyancat@upc.edu.cn (Z. Yan), Xiao.tiancun@chem.ox.ac.uk (T. Xiao).

0169-4332/$ – see front matter © 2012 Elsevier B.V. All rights reserved.
http://dx.doi.org/10.1016/j.apsusc.2012.05.078

oxide (ZnO) is also one of the most widely investigated materials for its unique catalytic, optical and electronic properties and many promising applications in environmental and energy areas [8,9]. Similarly, coupling TiO_2 with ZnO as a complex system (ZnO/TiO_2) has attracted much attention [20–22]. It is reported that this system can considerably improve the photocatalytic activity of TiO_2, which is attributed to the enhancement of the charge carrier separation due to the different energy band gap position of TiO_2 and ZnO, leading to the formation of a cascadal structure [21,22].

On the basis of the discussion above, the mixed oxides of two semiconductors (e.g. ZnO/TiO_2 and SnO_2/TiO_2) as coupling system have attracted extensive interests, and the catalyst samples have been also intensely produced by a variety of synthetic routes [17–22]. Here, we report on the synthesis of $SnO_2/ZnO/TiO_2$ heterojunctions through combining TiO_2 with both SnO_2 and ZnO by two simple methods: one is a modified sol–gel technique and the other is solid state synthesis. Our findings suggest that incorporation of SnO_2 and ZnO into TiO_2 as a complex system can extend the spectral response to the visible region and that the photocatalytic activity is greatly enhanced due to the promotion of the electron transfer through the interfacial potential gradient in the hybrid structure. Moreover, the effect of different Sn and Zn dopant concentration on the structural changes of coupling system such as the phase formation, the crystalline phase and the optical absorption, as well as the surface property was systematically studied. The liquid-phase photocatalytic degradation of Methyl Orange (MO) is chosen as a model reaction to evaluate the catalytic activity of the synthesized materials.

2. Experimental

2.1. Materials

All chemicals were used as received without further purification. Analytical grade tetrabutyl orthotitanate ($C_{16}H_{36}O_4Ti$, >97% Fluka Chemicals), tin tetrachloride pentahydrate ($SnCl_4{\cdot}5H_2O$) and zinc acetate dihydrate ($(CH_3COO)_2Zn{\cdot}2H_2O$) were utilized in the synthesis of composite photocatalyst by sol–gel method. Zinc oxide (ZnO, 99.99%, Aldrich), tin oxide (SnO_2, 99.99%, Aldrich) and titanium dioxide powders (TiO_2, 99.7%, Aldrich) were used in the synthesis of composite photocatalyst by the solid-state method.

2.2. Preparation of $SnO_2/ZnO/TiO_2$ composite photocatalyst

Sol–gel and solid-state methods were adopted to synthesize $SnO_2/ZnO/TiO_2$ composite system in the present work. The sol–gel synthesis method was modified compared to those reported previously [19]. In brief, 0.02 mol tetrabutyl orthotitanate were added dropwise into 50 ml absolute ethanol to give a solution which was then vigorously stirred for 20 min at room temperature. The desired amounts of $SnCl_4{\cdot}5H_2O$ and $(CH_3COO)_2Zn{\cdot}2H_2O$ (the molar ratio of Sn to Zn was 1:1) were then added in the reaction mixture while stirring continuously for 60 min until the Sn and Zn dopant dissolved. An amount of 2 mL of deionized water was then dropped into the above solution. Afterwards, the resultant solution mixture was maintained at room temperature with continuous stirring for 24 h to form a gel which was then aged for 12 h at room temperature. After being dried at 80 °C overnight, the as-prepared $SnO_2/ZnO/TiO_2$ samples were obtained and then annealed at 400, 500 and 600 °C for 3 h to give a yellowish material. The resultant composite materials coupled with different Zn and Sn contents by adjusting the molar ratio of Sn(Zn) to Ti from 0.05 to 0.20 were named as SG-0.05, SG-0.10, SG-0.15 and SG-0.20, respectively.

The solid-state preparation method was similar to those reported elsewhere [24]. In a typical procedure, TiO_2, SnO_2 and ZnO powders weighed in the desired ratio (the weight ratio of SnO_2 and ZnO to TiO_2 is 3 wt%, 6 wt% and 9 wt%) and placed together in an agate mortar. The resulting mixture was transferred into an alumina boat and kept at 900 °C in air for 10 h. The heated mixture was then removed from the oven and allowed to cool to room temperature naturally. The as-synthesized samples were marked as SS-3wt%, SS-6wt% and SS-9wt%, respectively. For comparison, the reference samples (undoped TiO_2, Zn/Ti-6wt% and Sn/Ti-6wt%) were prepared using the same approach.

2.3. Material characterization

X-ray diffraction (XRD) patterns of the composite samples were recorded on a Philips X-PeRT Pro Alpha 1 diffractometer operating with Cu Kα radiation (λ = 1.5406 Å) at a tube current of 40 mA and a voltage of 45 kV. Data were collected over 2θ values from 20° to 80° at a rate of 1°/min. The X-ray photoelectron spectroscopy (XPS) measurements were carried out using a Perkin-Elmer RBD upgraded PHI-5000C ESCA system with monochromatic Mg Kα excitation and a charge neutralizer. All bonding energies were calibrated to the C 1s peak at 284.8 eV of the surface adventitious carbon. Laser Raman spectra were obtained using a Perkin-Elmer RamanStation 400F Raman spectrometer. UV–vis diffuse reflectance spectra were recorded in a Perkin Elmer Lambda 750S UV/vis spectrometer equipped with an integrated sphere. The geometry and morphology of the $SnO_2/ZnO/TiO_2$ composite material were investigated with JSM840F scanning electron microscopy (SEM). The thermogravimetric analysis (TGA) was performed using TGA Q50 instrument (TA Instrument, United States) under air and N_2 atmosphere, respectively, and the heating rate was 10 °C min^{-1} from room temperature to 900 °C.

2.4. Photocatalytic test

Photocatalytic reactions were conducted in an open reactor with a cooling-water-cycle system keeping the reaction temperature constant. The light source was a 300 W Xenon lamp (Trusttech, Beijing, China), emitting UV and visible light simultaneously. For visible light measurements, a 400 nm cut-off glass filter was mounted before the output of light source to remove UV light and admit only visible light to enter into the reactor. The synthesized $SnO_2/ZnO/TiO_2$ composite catalyst (150 mg) was suspended in 150 ml of Methyl Orange (MO, 10 ppm) solution. Before the photoreaction, the suspension was stirred in the dark for 60 min to make sure the mixture had achieved adsorption/desorption equilibrium; then 3 ml of the solution was taken from the reactor every 30 min, the sample powder was separated from the solution by a centrifugation method. Concentration of MO was determined by UV–vis spectrophotometer. The UV photocatalysis test was performed in the same reactor; a 300 W Xenon lamp without UV glass filter was used as illuminating source. Typically, 50 mg composite catalyst and the MO aqueous solution (50 ml, 10 ppm) were added into the reaction system. All of suspensions were magnetically stirred in dark for 60 min to ensure the establishment of adsorption/desorption equilibrium of MO before the irradiation. After 40 min irradiation, the light source was switched off; 3 ml of the solution was taken out and centrifuged to remove the catalysts. The remaining transparent liquid was analyzed in a UV–vis spectrophotometer. It should be worthy noted that no sacrificial agent and oxygen were added into the solution during the reaction process.

3. Results and discussion

Fig. 1 shows the XRD data of solid state synthesized $SnO_2/ZnO/TiO_2$ composite catalysts with different amount of SnO_2

and ZnO combined including the data for only SnO_2 coupled TiO_2 and only ZnO coupled TiO_2 catalysts, used here as a reference, which has mixture of rutile TiO_2 and impurity phase such as SnO_2 or ZnO crystalline. Compared to the reference samples, the TiO_2 in the composite system shows a clear set of diffraction peaks characteristics of rutile phase for all samples. Moreover, the ZnO and rutile SnO_2 crystalline phase were observed within each sample. The inset of Fig. 1 shows the position change of the peak located at 2θ of 27.6°. Compared to the undoped TiO_2, a shift of the rutile TiO_2 (1 1 0) diffraction peaks towards lower 2θ angles with increasing Sn and Zn doping content was observed, which indicates that the Sn ions might incorporate into the TiO_2 lattice by the substitution of Sn onto Ti sites, leading to the expansion of the TiO_2 unit cell [24]. The SS-3wt% specimen shows a more obvious shift in the diffraction peak than other catalysts. This maybe due to the smaller grain size of the SS-3wt% powder, whereby the dissolution of SnO_2 and ZnO in TiO_2 is more significant than that of SS-6wt% and SS-9wt% powder.

Fig. 2 shows the X-ray diffraction patterns of SnO_2/ZnO/TiO_2 composite semiconductors synthesized by sol–gel method, the calcinations temperatures were 400 °C, 500 °C and 600 °C, respectively. It can be seen from Fig. 2(a) that the composite photocatalyst annealed at 400 °C exhibit pure anatase structure of TiO_2 at low Sn and Zn doping level (SG-0.05), no other phases were detected in the SG-0.05 heterojunctions. With the increase of the metal cations doping level, the SG-0.10 mainly has anatase structure, with a minor content of rutile structure. Further increasing the Sn(Zn) doping content, the main (1 1 0) Bragg peak of rutile is observed to become sharper and more intense, indicating that the formation of a large amount of rutile structure in the SnO_2/ZnO/TiO_2 composite catalyst. Moreover, a strong diffraction peak at around 26.6° was observed in the XRD patterns of SG-0.20 sample indicating the presence of a small amount of rutile SnO_2.

Fig. 2(b) shows the XRD data of SnO_2/ZnO/TiO_2 composite semiconductors annealed at 500 °C. It can be observed that the SG-0.05 sample has anatase as the dominant phase, and the main structure of SG-0.10 sample is still anatase structure, while a weak peak appears at around 27.2°, indicating the formation of a small amount of rutile phase. Compared with SG-0.10, the SG-0.15 sample heated at 500 °C shows a main rutile structure, with some anatase peaks remaining. Whereas, a pure rutile phase is observed in SG-0.20 sample, suggesting that the phase transition from anatase to rutile in the sample occurs. Besides the diffraction peaks for anatase and rutile TiO_2, there are two new crystalline structures (rutile SnO_2 and $ZnTiO_3$, respectively) formed in SG-0.20 sample after annealing, which may be explained by that the tin and zinc atomic content have reached saturation in the lattice at higher doping level.

The XRD spectra of SnO_2/ZnO/TiO_2 composite semiconductors annealed at 600 °C shows that the significant structure change occurs compared with those of the composite photocatalyst annealed at 400 and 500 °C. As can be seen from Fig. 2(c), the SG-0.05 sample shows a mixture of anatase and rutile phase, in addition to the impurity peaks corresponding to $ZnTiO_3$ that are also present in the composite SnO_2/ZnO/TiO_2 sample. With the increase of tin and zinc doping level, the diffraction peaks corresponding to anatase TiO_2 disappeared and only rutile TiO_2 as well as $ZnTiO_3$ phase was observed for the SG-0.15 sample, implying the anatase structure is completely transformed into rutile phase. Interestingly, we also observed the significant diffraction peaks of rutile phase SnO_2 in the XRD spectra of the SG-0.20 sample except for the TiO_2 and $ZnTiO_3$ structure.

On the basis of the above analysis, it could be found that the Sn and Zn ions doped in TiO_2 can promote the phase change from anatase to rutile TiO_2 in the range of annealing temperature from 400 °C to 600 °C. Moreover, higher annealing temperature (600 °C) not only leads to the formation of the impurity such as $ZnTiO_3$, but also favors the growth of rutile structure and gives SnO_2/ZnO/TiO_2 catalysts with larger particle size (Table S1). This finding is in accordance with the previous XRD results. Thus, a fine control of calcination temperature is crucial for obtaining a pure SnO_2/ZnO/TiO_2 heterostructure.

Raman spectroscopy was used to further evaluate the phase components of SnO_2/ZnO/TiO_2 catalysts prepared by different synthesis routes in this work. According to the previously reported data [25], anatase TiO_2 has six Raman bands at 144 cm^{-1} (E_g), 197 cm^{-1} (E_g), 399 cm^{-1} (B_{1g}), 513 cm^{-1} (A_{1g}), 519 cm^{-1} (B_{1g}) and 639 cm^{-1} (E_g). Rutile TiO_2 and SnO_2 belong to the same space group $D_{4h}(P4_2/mnm)$ and indicate four Raman active vibrational modes, $A_{1g} + B_{1g} + B_{2g} + E_g$ [26]. Fig. 3(a) shows the Raman spectra of SS-3wt%, SS-6wt% and SS-9wt%, and the Raman spectra of Sn/Ti-6wt% as well as Zn/Ti-6wt% for comparison. It can be observed that the main features of the Raman spectra of all SnO_2/ZnO/TiO_2 samples

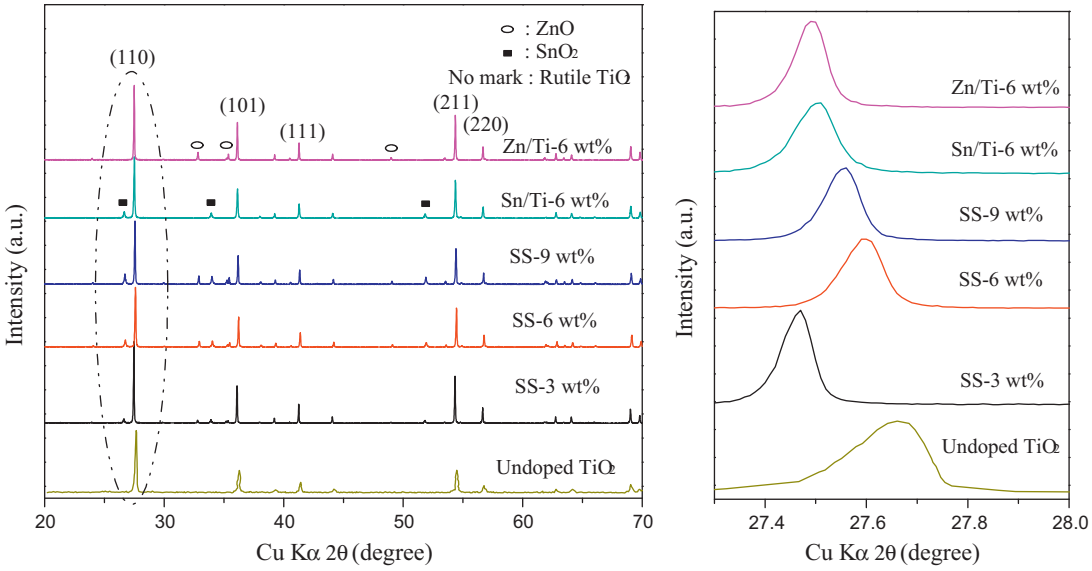

Fig. 1. X-ray diffraction patterns of solid state synthesized SnO_2/ZnO/TiO_2 composite catalysts with different amounts of SnO_2 and ZnO content. The inset shows the magnification of the diffraction peak around 27.6°.

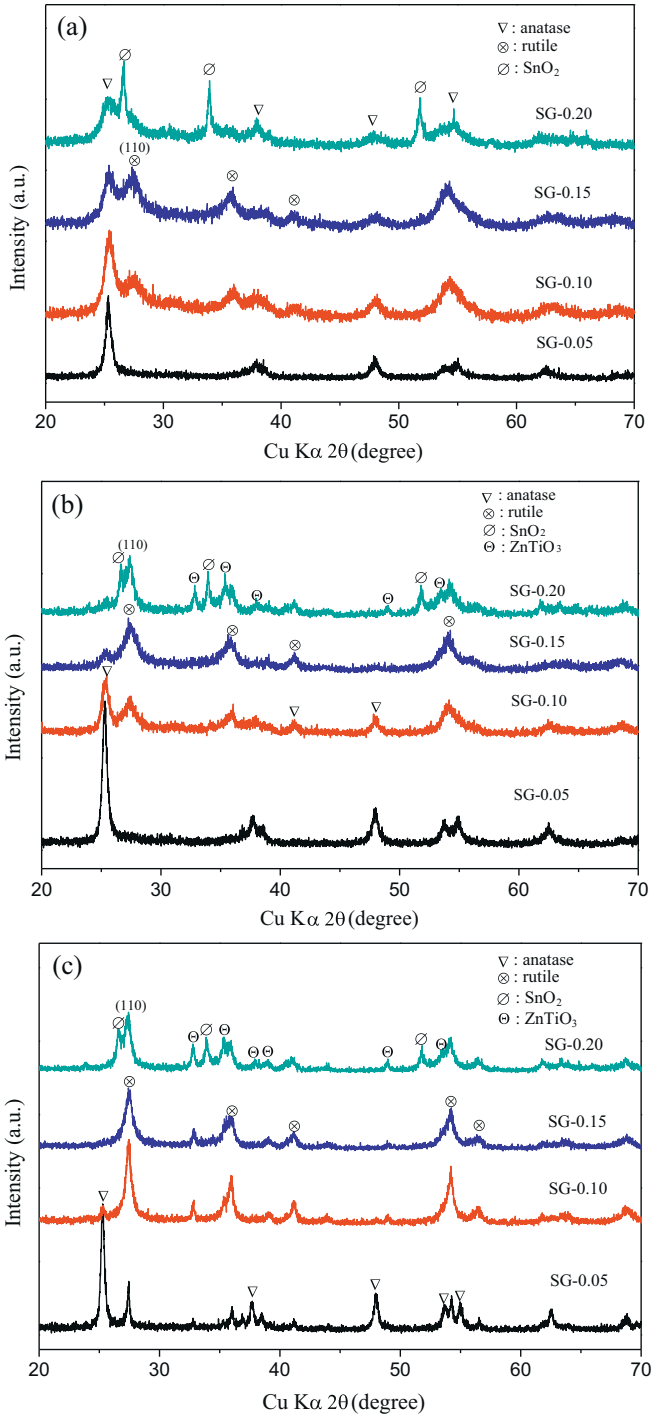

Fig. 2. X-ray diffraction patterns of sol–gel synthesized SnO_2/ZnO/TiO_2 composite catalysts with different amounts of SnO_2 and ZnO coupling and different calcinations temperatures: (a) 400 °C, (b) 500 °C and (c) 600 °C.

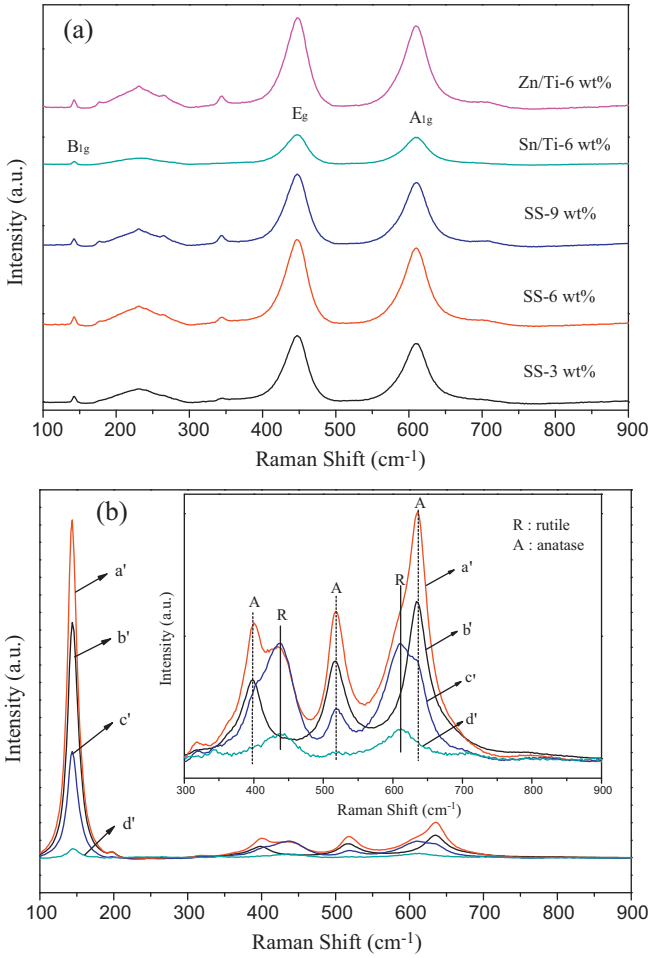

Fig. 3. Raman spectra of SnO_2/ZnO/TiO_2 composite catalysts with different amounts of SnO_2 and ZnO loading: (a) catalysts synthesized by solid state method and (b) catalysts synthesized by sol–gel method; the inset is the magnification of the Raman shift range from 300 cm^{-1} to 900 cm^{-1}: (a′) SG-0.05, (b′) SG-0.10, (c′) SG-0.15 and (d′) SG-0.20; these samples were annealed at 500 °C for 3 h.

are very similar, which all show the characteristic Raman bands of the rutile phase, with no evidence for the corresponding bands of the anatase phase, this finding is in accordance with the result of the X-ray diffraction measurements. The broad peak around 235 cm^{-1} is a combination band [26], and the B_{2g} vibration, located at 826 cm^{-1} is not detected owing to its weak intensity. In addition, the bands corresponding to SnO_2 and ZnO are not observed.

In Fig. 3(b), we show the Raman spectra of SnO_2/ZnO/TiO_2 catalysts synthesized by sol–gel methodology, and the obtained samples were annealed at 500 °C for 3 h in air. Here, it can be seen that all Raman spectra of composite catalyst samples exhibit rather similar spectra, four well-defined bands at 144, 399, 514 and 639 cm^{-1} were observed, which are characteristics of anatase structure [25]. Interestingly, as the Sn(Zn) dopant content increases, the intensity of main Raman band at 144 cm^{-1} assigned to anatase TiO_2 gradually reduced, indicating a lower crystallinity and small amount of anatase TiO_2 for the composite photocatalysts. The inset of Fig. 3(b) shows the localized profile of Raman spectra range from 300 cm^{-1} to 900 cm^{-1}, which can provide more information of phase evolution of the catalyst materials. Besides the characteristic Raman peaks of anatase TiO_2 (marked as "A"), two peaks at 447 and 612 cm^{-1} (marked as "R") were observed [6], which are attributed to the presence of rutile structure in samples SG-0.10 and SG-0.15, implying that two-phase co-exist with predominance of the rutile phase in the heterojunctions. When the Sn(Zn) doping content increased, only rutile phase was observed in sample SG-0.20, it is therefore concluded that the Sn and Zn co-doping could induce the phase change from anatase to rutile phase, which is in good agreement with those from XRD data. The main Raman bands at 776, 636, 574 and 490 cm^{-1} attributed to SnO_2 are all undetectable [27], indicating the metal ions either has been doped into the titania lattice and does not exist as a separate crystalline oxide phase, or maybe the bands assigned to SnO_2 are overlapped with the crystalline plane of TiO_2.

It is well known that the diffuse reflection spectroscopy is a powerful technique to detect the optical absorption properties of semiconductor and the information on its band gap. Fig. 4(a) shows the corresponding UV–vis diffuse reflectance spectra and the band-gap energies calculated from the adsorption edges of composite semiconductor samples prepared by solid-state method. For comparison, the reference sample Zn/Ti-6wt% and Sn/Ti-6wt% are also shown in Fig. 4(a). All the composite photocatalysts have a strong and broad absorption feature in the UV region (below 388 nm) due to the inter band electronic transitions [28]. Moreover, all the SnO_2/ZnO/TiO_2 catalysts including the reference samples show significant optical absorption in the visible region from 390 nm to 430 nm due to the characteristic of rutile structure TiO_2, which is formed after being annealed at 900 °C. The absorption profiles of the reference samples were similar, with peak at 415 nm (Zn/Ti-6wt%) and 416 nm (Sn/Ti-6wt%), which correspond to band gaps of 2.99 and 2.98 eV, respectively. In comparison with the reference samples, the band absorption in the spectra of the composite catalysts shows that TiO_2 combining Sn and Zn could result in a slight red-shift of absorption edge. Interestingly, a monotonic decrease in the UV–vis DRS spectra of composite samples was observed, indicating that the absorption threshold of the samples shift decreased with the increase of Sn and Zn dopants content. Fig. 4 shows that the absorption band edge shifted to 420 nm (2.95 eV) for the SS-3wt% sample, whereas when with 9 wt% Sn(Zn) co-doping, a shift in the optical absorption edge of TiO_2 into visible light region, at 417 nm, was observed, which correspond to a band gap of 2.97 eV. The results demonstrate that the degree of tin and zinc coupling affect the visible light absorption of TiO_2.

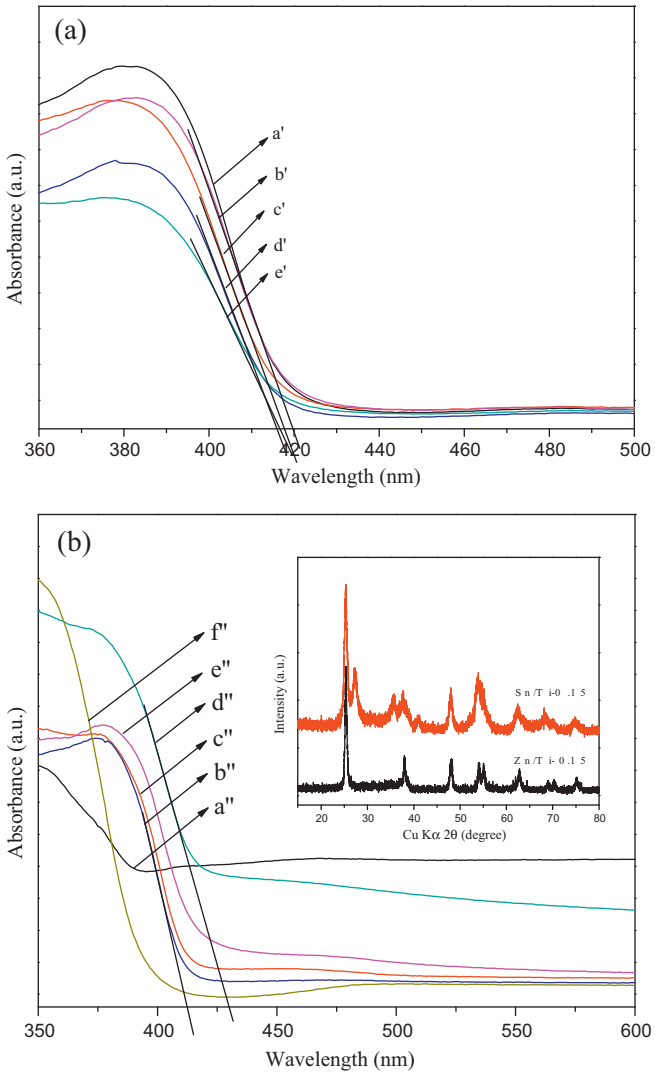

Fig. 4. Optical absorption spectra of SnO_2/ZnO/TiO_2 catalysts with different amounts of SnO_2 and ZnO loading. (a) Catalysts synthesized by solid state method: (a′) SS-3wt%, (b′) SS-9wt%, (c′) SS-6wt%, (d′) Zn/Ti-6wt% and (e′) Sn/Ti-6wt%. (b) Catalysts synthesized by sol–gel method: (a″) SG-0.05, (b″) SG-0.10, (c″) SG-0.15, (d″) SG-0.20, (e″) Sn/Ti-0.15 and (f″) Zn/Ti-0.15. The inset shows the corresponding XRD data of reference samples.

The diffuse reflectance UV–vis spectroscopic analysis has been carried out for the SnO_2/ZnO/TiO_2 heterojunctions prepared by sol–gel method and the reference Sn/Ti-0.15 and Zn/Ti-0.15 catalysts. Fig. 4(b) shows the corresponding UV–vis diffuse reflectance spectra (DRS) of the samples annealed at 500 °C for 3 h. It can be seen that the absorption thresholds of the reference samples show a significant difference. For the Zn/Ti-0.15 sample, there is a strong optical absorption at the wavelength range lower than 390 nm mainly attributed to the electron transitions from the valence band to conduction band, and the visible light absorption is not observed, suggesting the reference Zn/Ti-0.15 sample is pure anatase structure, which is consistent with XRD analysis (the inset of Fig. 4(b)). In contrast, the sample, Sn/Ti-0.15 presents an apparent visible light absorption in the range of 400–430 nm due to the presence of a small amount of rutile phase TiO_2 in this sample (the band gap of rutile TiO_2 is 3.0 eV), which has been confirmed by the X-ray diffraction data that Sn-only doping can accelerate the transition of TiO_2 from anatase to rutile. In comparison with the reference catalysts, the optical absorption edges of SnO_2/ZnO/TiO_2 samples locate in the range of 412–430 nm, corresponding to a band gap energy (E_g) of approximately 3.0–2.88 eV. It also can be seen that the band gap decreases monotonically with increasing Sn and Zn concentration, implying that the level of Sn and Zn co-doping has a remarkable effect on the optical absorption of SnO_2/ZnO/TiO_2 composite catalysts. There is, moreover, a very broad and flat absorption tail that extends across much of the visible light region down to 600 nm observed for SG-0.05 and SG-0.20 photocatalysts, which is reasonable because of less Sn cations occupying sites at surface or grain boundary interfaces [24].

XPS analysis was performed to investigate into the surface composition and the existing chemical states of Sn and Zn ions in SnO_2/ZnO/TiO_2 composite catalysts. Fig. 5 shows the typical XPS results of SG-0.15 catalyst annealed at 500 °C for 3 h. As can be seen from Fig. 5(a), the X-ray photoelectron spectroscopy survey spectrum indicates that the SG-0.15 sample contains predominantly O, Ti, Sn, Zn and C elements. It is thought to be the residual carbon from the organic precursor solution and the adventitious carbon from the XPS instrument itself are the main reason to cause the presence of C element. The O 1s XPS spectrum is shown in Fig. 5(b). It can be observed that the broad peak of O 1s is asymmetric, and that can be fitted by two peaks at 528.8 eV and 530.1 eV, indicating there are two independent chemical states for O within SG-0.15. The low binding energy (BE) of 528.8 eV is ascribed to the lattice oxygen of TiO_2 (OL) [29], and the peak located at high binding energy (530.1 eV) for O element can be corresponded to surface hydroxyl groups such as Ti–OH and Ti–O–O resulting from chemisorbed water (OH) [30]. In Fig. 5(c), the Ti 2p XPS spectra of SG-0.15 has two peaks centered at 458.5 and 463.9 eV, which are attributed to the Ti $2p_{3/2}$ and $2p_{1/2}$ spin–orbital splitting photoelectrons in Ti^{4+}, these data agree well with previously reported XPS data for TiO_2 [22]. Additionally, the band located at the low binding energy (458.5 eV) is broad and asymmetric, demonstrating that there are at least two kinds of Ti chemical states. After curve fitting, besides the peak corresponding to the Ti^{4+}, the other peak at 457.4 eV were identified, suggesting the existence of Ti^{3+} in the composite catalyst [31,32], and the formation of Ti^{3+} shows the presence of lots of oxygen vacancies during the doping process.

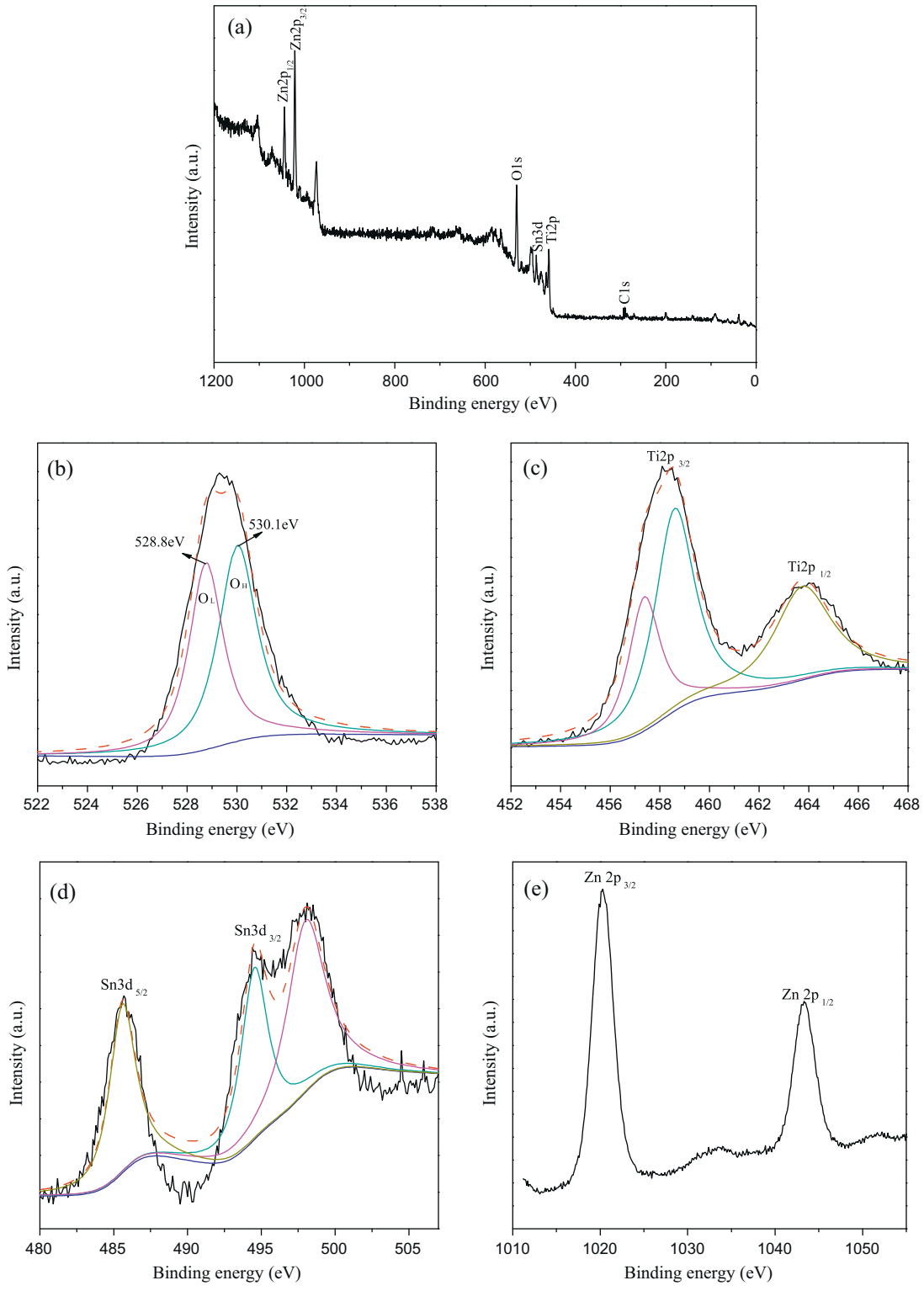

Fig. 5. The XPS spectra of SG-0.15 sample: (a) the survey spectra, (b) O 1s, (c) Ti 2p, (d) Sn 3d and (e) Zn 2p.

Fig. 5(d) shows the Sn 3d XPS spectra of SG-0.15 annealed at 500 °C for 3 h. The binding energy of 485.6 and 494.6 eV is ascribed to Sn $3d_{5/2}$ and Sn $3d_{3/2}$, respectively, assigned to Sn in 4+ state species [23–29]. According to the literature [23], the peak position corresponding to Sn $3d_{3/2}$ is centered between those of Sn $3d_{3/2}$ (485.0 eV) in metallic Sn and Sn $3d_{3/2}$ in SnO_2 (486.6 eV), which suggests the Sn^{4+} ions incorporated into lattice of TiO_2 and cause a small structural distortion in SG-0.15 sample. Besides, it is worthy to be noted that the peak at 499.0 eV is due to a plasmon peak (P) in clean Sn metal [33].

The XPS spectra of Zn 2p region was shown in Fig. 5(e). The doublet peak corresponding to Zn $2p_{3/2}$ and Zn $2p_{1/2}$ were observed. The peak positions of Zn $2p_{3/2}$ and Zn $2p_{1/2}$ is located at 1020.4 and 1043.4 eV, respectively, and the binding energy distance between Zn $2p_{3/2}$ and Zn $2p_{1/2}$ is 23.0 eV, indicating the Zn species mainly existed as the chemical state of Zn^{2+} [34], which coincide with the

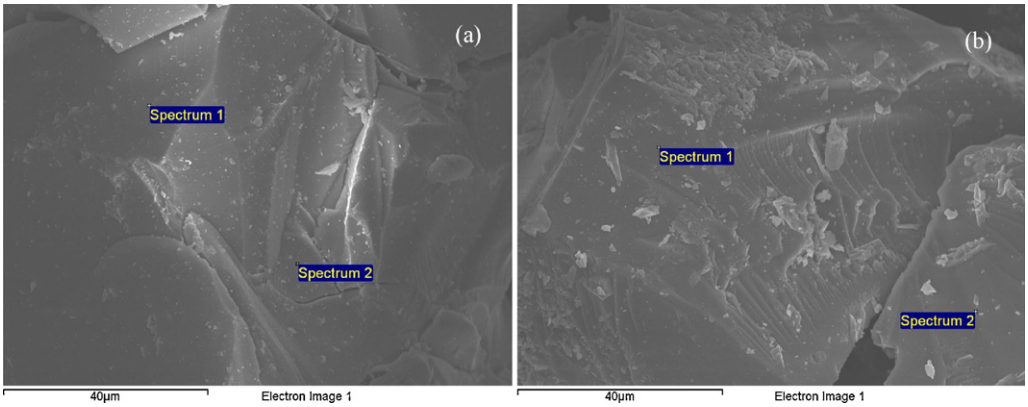

Fig. 6. SEM images of SG-0.05 (a) and SG-0.15 sample (b). All the samples annealed at 500 °C.

Zn^{2+} position with oxygen. It is known that the radius of Zn^{2+} is 0.88 Å, which is larger than that of Ti^{4+} [22]. Thus, the Zn^{2+} ion is very hard to replace the Ti^{4+} site and occupy its position in theory during the preparation. It is therefore thought that the Zn ions either possibly resided over the surface of catalyst particle with a form of ZnO cluster or the formation of $ZnTiO_3$ on the surface of SG-0.15.

Fig. 6 shows the representative SEM images of SG-0.05 and SG-0.15 samples, respectively. It can be seen that the typical morphology observed in all of the preparations is composed of solid particle structure. Comparing these two SEM images, it is found that the surface of SG-0.05 is smooth, in contrast to the rugged surface of SG-0.15 sample, no noticeable changes have been found for the catalysts with various Sn(Zn) doping level. The EDX analysis was also employed to detect the chemical compositions of the SnO_2/ZnO/TiO_2 composite catalysts. Table S2 lists the chemical compositions and concentration of SnO_2/ZnO/TiO_2 samples with different Sn(Zn) content. The results of EDX analysis clearly reveal that the SG-0.15 mainly composed of Ti, O, C, Zn and Sn, indicating that the as-prepared composite catalyst have the well-mixed heterojunctions, consistent with XPS and XRD finding. However, zinc element was not observed in the SG-0.05 sample. This is probably due to the zinc content is quite low and dispersed unevenly on SnO_2/ZnO/TiO_2 when the Zn doping level is 0.05.

Fig. 7 shows the TGA curve for the SG-0.15 sample, which was performed in the N_2 and air atmosphere, respectively. Here, both of the TGA spectra are rather similar: five peaks appeared in the TGA curve, the mass loss of SG-0.15 can be identified in the TG curve. A broad endothermic peak existed in the range of 20–160 °C due to the desorption of the physical adsorbed water and ethanol [35], and the mass loss is greatest in the stage, which is up to 9%. The sharp endothermic at about 224 °C was observed owing to the decomposition of unhydrolyzed $Ti(OBu)_4$ remained in the TiO_2 xerogel powders [36], and the mass loss was about 7.5%. In the range of 300–500 °C, there were two small peaks which can be assigned to the oxidation of remnant organic compounds and the phase transformation process from amorphous to anatase phase [29,37]. The mass loss process is quite slow in this stage, only 4% mass loss was observed. A small and broad peak at around 590 °C corresponds to the thermal effect caused by the phase transition from anatase to rutile TiO_2, and no mass loss was observed [29]. The results further confirmed that the Sn and Zn doped in TiO_2 could favor the phase change of anatase to rutile. (Generally, most pure TiO_2 particles were transformed into rutile above 700 °C.)

In order to test the photocatalytic activity of the as-prepared SnO_2/ZnO/TiO_2 composite catalysts, we chose Methyl Orange (MO) as a model pollution to evaluate the catalytic behavior of the samples. Fig. 8(a) shows the degradation of MO dye over the composite catalysts annealed at 500 °C for 3 h, including data for the reference samples, which was illuminated with a 300 W Xe lamp irradiation equipped with a cut-off glass filter ($\lambda > 400$ nm). It is clear that the MO solution is very stable and no decomposition in absence of photocatalysts can be observed at all. However, the use of the composite catalysts could lead to an obvious inactivation of MO without adding any sacrificial agent, owing to the enhanced transfer of charge carriers and light absorption capability of the composite catalyst. It can also be seen that the co-doping level affects the photocatalytic activity, with the SG-0.05 sample displaying the highest photocatalytic activity under visible light irradiation, on which more than 45% MO was decomposed in 300 min reaction time; this is due to the well crystallized anatase TiO_2 could facilitate the transfer of photogenerated electron from bulk to surface

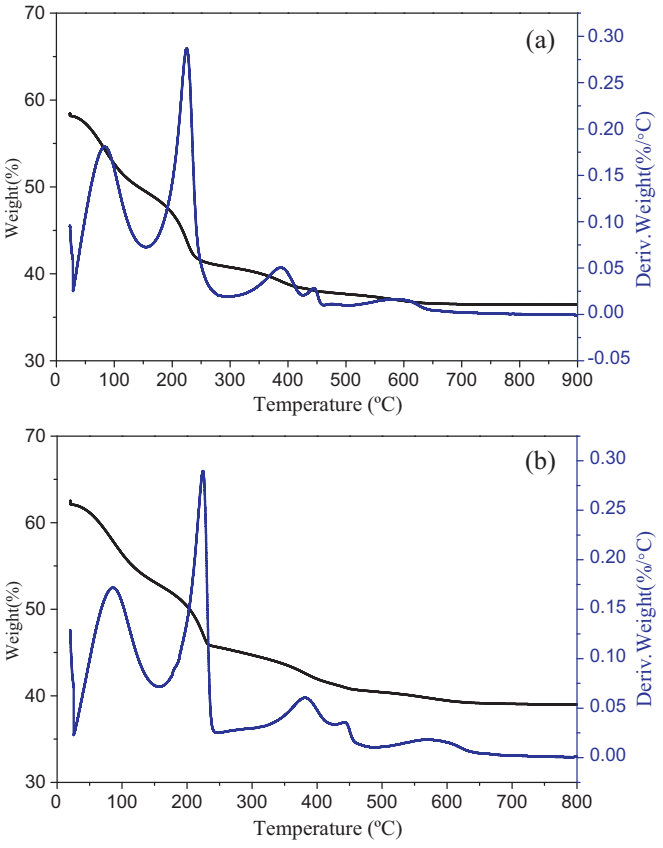

Fig. 7. TGA curves of SG-0.15 sample: (a) N_2 atmosphere and (b) air atmosphere.

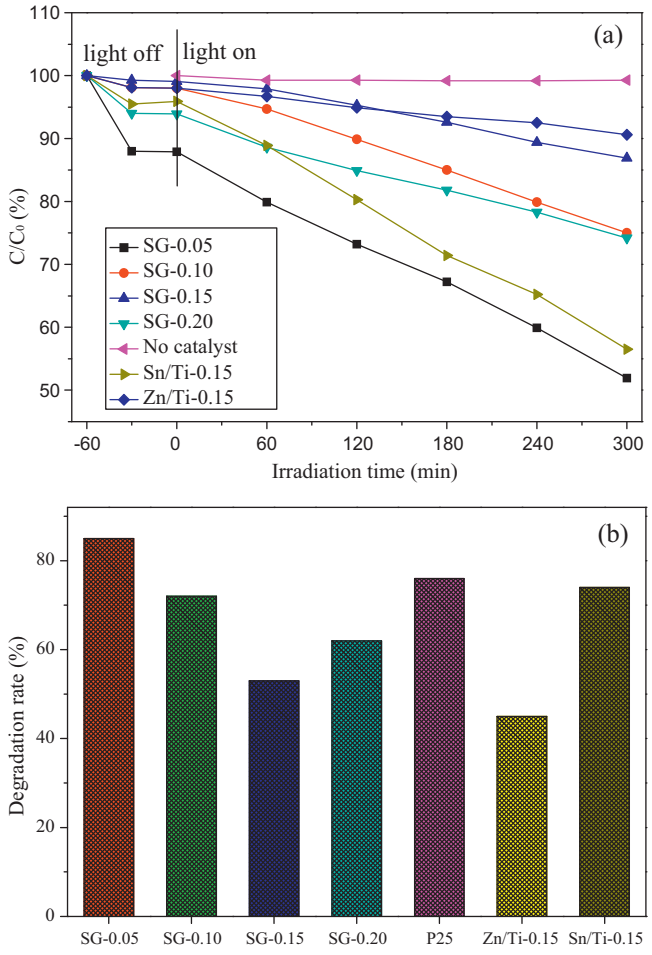

Fig. 8. Photocatalytic degradation of Methyl Orange over the sol–gel synthesized $SnO_2/ZnO/TiO_2$ composite catalysts: (a) under visible light irradiation ($\lambda > 400$ nm), the samples were calcined at 500 °C for 3 h and (b) under UV light irradiation (reaction time: 40 min).

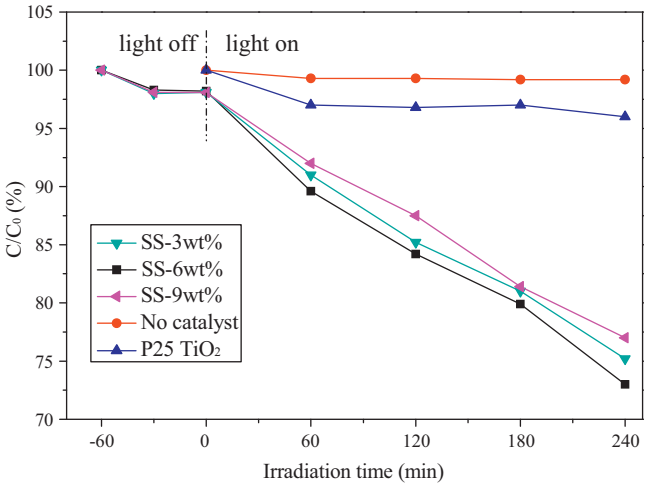

Fig. 9. Photocatalytic activity curves of degradation of Methyl Orange over SS-6wt% catalysts and P25 TiO_2 under visible light irradiation ($\lambda > 400$ nm).

and thus inhibit the recombination of electron–hole pairs. The SG-0.15 sample showed lower photodegradation performance with a MO conversion of 13% under the same visible light irradiation time, which only showed a little better activity than Zn/Ti-0.15. The photodegradation of MO on Zn/Ti-0.15 can be attributed to dye sensitized photocatalysis since Zn/Ti-0.15 has no optical absorption in the visible light region (see Fig. 4).

Fig. 8(b) shows the results obtained from the photocatalytic experiment for the inactivation of MO over the composite catalysts annealed at 500 °C for 3 h and reference samples under UV light irradiation. It can be seen that all the photocatalysts showed some activity under UV light irradiation, and the SG-0.05 sample exhibits the highest photocatalytic activity among these samples; the degradation yield of SG-0.05 approaches to 85% after 40 min irradiation. Besides the SG-0.05 sample, the degradation rates of SG-0.10, SG-0.15 and SG-0.20 are poorer than that of bare TiO_2 (P25). Among the three samples, the SG-0.15 sample demonstrates much worse catalytic performance, both under UV and visible irradiations, this may result from the synergic effect of the small surface area, low MO absorption capability and low crystallinity of the sample [20]. On the other hand, the formation of the rutile phase at the high Sn–Zn doping level is also an important factor to result in a significant decrease of the catalytic decomposition of MO for the SG-0.15 sample. In Fig. 9, we show the visible-light-induced photocatalytic activity for the degradation of MO over $SnO_2/ZnO/TiO_2$ heterojunctions synthesized by solid-state method. It can be seen that P25 TiO_2 cannot be activated by visible light due to its large energy band gap, and the SS-6wt% sample showed enhanced photocatalytic activity under visible light, with a MO conversion of 27% can be observed after 240 min irradiation.

We have also attempted to understand the enhancement of the visible light-induced photocatalytic activity of $SnO_2/ZnO/TiO_2$ composite semiconductor. As previously reported [2,18,34,39,40],

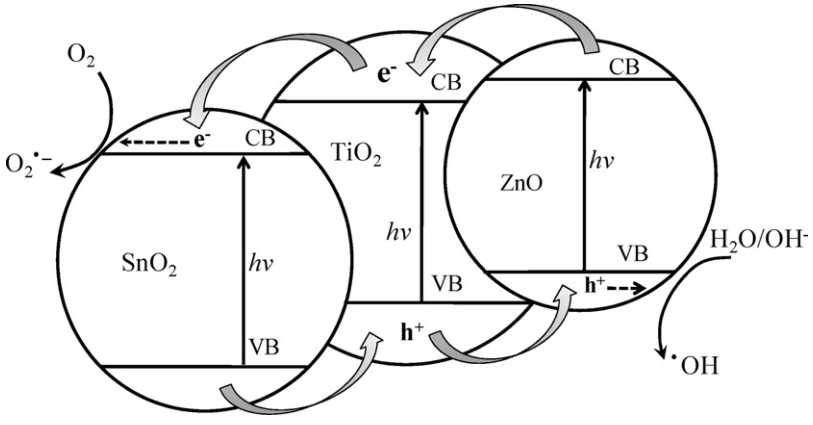

Fig. 10. Schematic energy band structure and electron–hole pair separation process of $SnO_2/ZnO/TiO_2$ composite semiconductor system.

there are several factors accounting for the enhancement mechanisms of catalytic activity of composite catalysts. Firstly, the higher specific surface area of SnO_2/ZnO/TiO_2 heterojunctions would provide stronger adsorption ability of the catalytic surface toward target molecules and better ability to photoexcite the electron–hole pairs in the active sites [38]. Moreover, the special band structure of SnO_2/ZnO/TiO_2 heterojunctions plays vital role in the enhancement of photocatalytic activity for the discoloration of MO solution. Therefore, a tentative mechanism for the band configuration at the contacted interface of SnO_2/ZnO/TiO_2 material was proposed. Fig. 10 shows the schematic diagram of the energy band gap and the charge transfer in the SnO_2/ZnO/TiO_2 composite semiconductor system. As we have known, the band gap of SnO_2, ZnO and TiO_2 is 3.8 eV, 3.37 eV and 3.2 eV, respectively, suggesting that these semiconductors have different electron affinity and band configuration. TiO_2 has the conduction band (CB) edge that is below that of ZnO and above that of SnO_2. Thus, a "staggered" type II heterojunction at the interface of the SnO_2/ZnO/TiO_2 is formed. Under UV or visible light irradiation, electrons in the valence band (VB) of TiO_2 were excited to its conduction band (CB), while the hole remains in VB, and due to the Fermi energy level of TiO_2 is higher than that of SnO_2, the electrons in CB was driven by the potential energy to transfer to the CB of SnO_2. Conversely, the photogenerated hole can move from VB of SnO_2 to that of TiO_2 [39,40]. It can be seen that in this process the electrons and holes were separated efficiently at the SnO_2/TiO_2 interfaces, resulting in a large number of charge could participate in decolorized reaction and enhance quantum efficiency. Similarly, when the electron–hole pairs are generated in the ZnO, electrons can be separated from holes by migrating to TiO_2 and then SnO_2 in a cascadal way along the potential gradient as shown in Fig. 10 [21,34]. Consequently, the electrons eventually localized the conduction band of SnO_2, reducing O_2 to form superoxide ions ($O_2^{\bullet -}$), and the hole located in the valence band of ZnO then reacts with hydroxyl group to produce the hydroxyl radical ($^{\bullet}OH$), which are responsible for the discoloration of the Methyl Orange in the photoreaction.

On the basis of the above analysis, we tentatively concluded that combining three semiconductors with different energy levels to form a ternary hybrid catalyst can facilitate the transfer of the electrons, reduce the recombination probability and increase the charge carrier lifetime, as a consequence of the enhancement of the photocatalytic activity for SnO_2/ZnO/TiO_2 samples. Indeed, enhanced activity was observed for the synthesized SG-0.05 heterojunction, indicating that the recombination of charge carrier is inhibited greatly among all the SnO_2/ZnO/TiO_2 samples.

4. Conclusions

In this work, two facile approaches, e.g. sol–gel method and solid-state method were developed to synthesize SnO_2/ZnO/TiO_2 composite semiconductor in this work. The XRD and Raman analysis reveals that incorporating SnO_2 and ZnO can promote the formation of rutile TiO_2, and also shows that these cations interdiffusion caused variations in the crystalline phase composition. The results of XPS exhibit Sn^{4+} ions can be doped into the TiO_2 lattice by substituting the Ti^{4+} ions, and Zn ions exist in the form of $ZnTiO_3$ or oxide on the surface of TiO_2. Regarding photocatalytic activity for the degradation of Methyl Orange, an obvious beneficial effect is observed in all SnO_2/ZnO/TiO_2 composite catalysts. This induces favorable charge separation and inhibits the recombination of electron–hole pairs, thereby facilitating the electron transfer from bulk to surface within the composite structure. In addition, the composite catalysts synthesized by sol–gel method show a much stronger photocatalytic activity than that of the catalysts synthesized by solid-state method.

Acknowledgment

We thank the UK photocatalysis Network for their kind support.

Appendix A. Supplementary data

Supplementary data associated with this article can be found, in the online version, at http://dx.doi.org/10.1016/j.apsusc.2012.05.078.

References

[1] S.C. Hayden, N.K. Allam, M.A. El-Sayed, Journal of the American Chemical Society 132 (2010) 14406–14408.
[2] H. Kim, J. Kim, W. Kim, W. Choi, Journal of Physical Chemistry C 115 (2011) 9797–9805.
[3] F. Fresno, M.D. Hernández-Alonso, D. Tudela, J.M. Coronado, J. Soria, Applied Catalysis B: Environmental 84 (2008) 598–606.
[4] D.R. Baker, P.V. Kamat, Advanced Functional Materials 19 (2009) 805–811.
[5] Q. Zhang, W. Fan, L. Gao, Applied Catalysis B: Environmental 76 (2007) 168–173.
[6] G. Yang, Z. Jiang, H. Shi, M.O. Jones, T. Xiao, P.P. Edwards, Z. Yan, Applied Catalysis B: Environmental 96 (2010) 458–465.
[7] M. Batzill, U. Diebold, Progress in Surface Science 79 (2005) 47–154.
[8] Q. Zhang, C.S. Dandeneau, X. Zhou, G. Cao, Advanced Materials 21 (2009) 4087–4108.
[9] H.-M. Xiong, Journal of Materials Chemistry 20 (2010) 4251–4262.
[10] G. Yang, T. Xiao, J. Sloan, G. Li, Z. Yan, Chemistry – A European Journal 17 (2011) 1096–1100.
[11] G. Yang, Z. Jiang, H. Shi, T. Xiao, Z. Yan, Journal of Materials Chemistry 20 (2010) 5301–5309.
[12] W. Zhang, L. Zou, L. Wang, Applied Catalysis A: General 371 (2009) 1–9.
[13] G. Yang, Z. Yan, T. Xiao, Applied Surface Science 258 (2012) 4016–4022.
[14] F. Han, V.S.R. Kambala, M. Srinivasan, D. Rajarathnam, R. Naidu, Applied Catalysis A: General 359 (2009) 25–40.
[15] J. Nayak, S.N. Sahu, J. Kasuya, S. Nozaki, Applied Surface Science 254 (2008) 7215–7218.
[16] M. Niu, F. Huang, L. Cui, P. Huang, Y. Yu, Y. Wang, ACS Nano 4 (2010) 681–688.
[17] R. Sui, J.L. Young, C.P. Berlinguette, Journal of Materials Chemistry 20 (2010) 498–503.
[18] C. Wang, C. Shao, X. Zhang, Y. Liu, Inorganic Chemistry 48 (2009) 7261–7268.
[19] L.-C. Chen, F.-R. Tsai, S.-H. Fang, Y.-C. Ho, Electrochimica Acta 54 (2009) 1304–1311.
[20] C. Wang, B.-Q. Xu, X. Wang, J. Zhao, Journal of Solid State Chemistry 178 (2005) 3500–3506.
[21] Z. He, Y. Li, Q. Zhang, H. Wang, Applied Catalysis B: Environmental 93 (2010) 376–382.
[22] Y. Zhao, C. Li, X. Liu, F. Gu, H.L. Du, L. Shi, Applied Catalysis B: Environmental 79 (2008) 208–215.
[23] Y. Cao, T. He, L. Zhao, E. Wang, W. Yang, Y. Cao, Journal of Physical Chemistry C 113 (2009) 18121–18124.
[24] M.H. Harunsani, F.E. Oropeza, R.G. Palgrave, R.G. Egdell, Chemistry of Materials 22 (2010) 1551–1558.
[25] K. Yanagisawa, J. Ovenstone, Journal of Physical Chemistry B 103 (1999) 7781–7787.
[26] S.P.S. Porto, P.A. Fleury, T.C. Damen, Physical Review 154 (1967) 522–526.
[27] B.X. Huang, P. Tornatore, Y.-S. Li, Electrochimica Acta 46 (2000) 671.
[28] P. Du, J.A. Moulijn, G. Mul, Journal of Catalysis 238 (2006) 342–352.
[29] L. Jing, H. Fu, B. Wang, D. Wang, B. Xin, S. Li, J. Sun, Applied Catalysis B: Environmental 62 (2006) 282–291.
[30] J.G. Yu, H.G. Yu, B. Cheng, X.J. Zhao, J.C. Yu, W.K. Ho, Journal of Physical Chemistry B 107 (2003) 13871–13879.
[31] H. Liu, W. Yang, Y. Ma, J. Yao, Applied Catalysis A: General 299 (2006) 218–223.
[32] G. An, W. Ma, Z. Sun, Z. Liu, B. Han, S. Miao, Z. Miao, K. Ding, Carbon 45 (2007) 1795–1801.
[33] H. Ohno, Y. Kanzawa, Y. Yamane, Dental Materials Journal 2 (1983) 59–67.
[34] L. Jing, B. Xin, F. Yuan, L. Xue, B. Wang, H. Fu, Journal of Physical Chemistry B 110 (2006) 17860–17865.
[35] J. Yu, M. Zhou, B. Cheng, X. Zhao, Journal of Molecular Catalysis A: Chemical 246 (2006) 176–184.
[36] J.C. Yu, J.G. Yu, W.K. Ho, Z.T. Jiang, L.Z. Zhang, Chemistry of Materials 14 (2002) 3808–3816.
[37] S. Mahanty, S. Roy, S. Sen, Journal of Crystal Growth 261 (2004) 77–81.
[38] G. Marci, V. Augugliaro, M.J. Lopez-Munoz, C. Martin, L. Palmisano, V. Rives, M. Schiavello, R.J.D. Tilley, A.M. Venezia, Journal of Physical Chemistry B 105 (2001) 1026–1032.
[39] F. Sayılkan, M. Asiltürk, P. Tatar, N. Kiraz, E. Arpaç, H. Sayılkan, Journal of Hazardous Materials 144 (2007) 140–146.
[40] R. Long, Y. Dai, G. Meng, B. Huang, Physical Chemistry Chemical Physics 11 (2009) 8165–8172.